





Article

AA7050 Al Alloy Hot-Forging Process for Improved Fracture Toughness Properties

Giuliano Angella ¹, Andrea Di Schino ², Riccardo Donnini ¹, Maria Richetta ³,
Claudio Testani ⁴ and Alessandra Varone ^{3,*}

¹ Istituto di Chimica della Materia Condensata e di Tecnologie per l'Energia (ICMATE), Consiglio Nazionale delle Ricerche (CNR), Via R. Cozzi, 20125 Milan, Italy; giuliano.angella@cnr.it (G.A.); riccardo.donnini@cnr.it (R.D.)

² Dipartimento di Ingegneria, Università degli Studi di Perugia, Via G. Duranti 93, 06125 Perugia, Italy; andrea.dischino@unipg.it

³ Dipartimento di Ingegneria Industriale, Università degli Studi Roma Tor Vergata, Via del Politecnico 1, 00133 Roma, Italy; richetta@uniroma2.it

⁴ Consorzio per la ricerca e lo sviluppo delle Applicazioni industriali del Laser E del Fascio elettronico e dell'Ingegneria di processo, materiali, metodi e tecnologie di produzione CALEF-ENEA CR Casaccia, Via Anguillarese 301, Santa Maria di Galeria, 00123 Rome, Italy; claudio.testani@consorziocalef.it

* Correspondence: alessandra.varone@uniroma2.it; Tel.: +39-0672597180

Received: 21 December 2018; Accepted: 8 January 2019; Published: 11 January 2019



Abstract: The conventional heat-treatment standard for the industrial post hot-forging cycle of AA7050 is regulated by the AMS4333 and AMS2770N standards. An innovative method that aimed to improve toughness behavior in Al alloys has been developed and reported. The unconventional method introduces an intermediate warm working step between the solution treating and the final ageing treatment for the high resistance aluminum alloy AA7050. The results showed several benefits starting from the grain refinement to a more stable fracture toughness KIC behavior (with an appreciable higher value) without tensile property loss. A microstructural and precipitation state characterization provided elements for the initial understanding of these improvements in the macro-properties.

Keywords: Al alloys; warm working; mechanical properties

1. Introduction

For AA7050, the AMS4333 and AMS2770N standards require cold working after solution heat treatment and prior to aging [1,2]. Moreover, the tensile properties of the heat-treatable aluminum alloys are improved by this process because of the pinning of the dislocation structures developed during the deformation, nucleation and refinement of the S' precipitates in Al-Cu-Mg alloys, θ' precipitates in Al-Cu alloys, and T1 precipitates in lithium-containing Al-Cu-Mg alloys [3]. Homogeneously distributed fine precipitates are responsible for the increased tensile properties compared to un-aged alloy [4].

A component with a complex geometrical shape made of an Al alloy is usually achieved by the closed-die forging of a billet. The 3D hot-forging process allows control of the metal flow, and hence the formation of the target microstructures in the component bulk. The components are usually manufactured to obtain a combination of strength, toughness and fatigue resistance [5]. Therefore, the directional properties of the crystal structure will meet the directional requirements of the service application. On the contrary, the open-die forging process permits the application of compression-force and the related deformation flows by means of axial pressing, and it is quite impossible to obtain a uniform volume and thickness deformation because of the forged components of 3D complex shapes.

Some forging experiments were carried out on an AA7050 aluminum alloy in agreement with AMS4333 requirements. In particular, it has to be noted that the AMS4333 standard introduces, after the solution treatment, an intermediate cold deformation step (5% max) before final aging to reach the optimum microstructure and precipitates distribution, improving tensile properties [6,7].

The alternative process, shown here, adopts an intermediate warm deformation step, instead of room temperature deformation between the quenching and ageing step, and is aligned with other literature attempts and techniques to improve strength for Al alloys [8,9]. For AA 2024 alloy, Garay-Reyes et al. [10] showed that the best properties are reached by a complex two-stage ageing treatment, where the solution heat treatment is followed by stretching at room temperature, a first aging step to T3 temper, warm working in the deformation range 5–15% at 463 K and a final aging treatment at 463 K [10]. Similar studies have been performed in 8XXX alloys [11].

AA7050 alloy belongs to the 7XXX family that is widely applied in aeronautical applications [12–14] because of a unique combination of strength and toughness. Relevant contributions to the knowledge of its hot deformation behavior are presented in [15–17]. Moreover, AA7050 represents one of the best performing alloys in the 7XXX aluminum family, for its good balance of high strength, corrosion resistance and toughness [18,19] achieved by controlling the recrystallisation phenomena during and after hot forming processes [20–25].

The aim of this paper was to investigate the mechanical properties resulting from the innovative heat and thermo-mechanical treatment (up-setting carried out at temperatures of 423 K and 473 K instead of room temperature as in the standard cycle) and to describe the introduced microstructural and precipitation state modification.

2. Materials and Methods

The examined material was AA7050 alloy, and its chemical composition is reported in Table 1.

Table 1. Nominal chemical composition of AA7050 alloy (wt %).

Elements	Al	Zr	Si	Fe	Cu	Mn	Mg	Cr	Zn	Ti
wt (%)	Bal.	0.12	<0.12	<0.15	2.30	<0.10	2.20	<0.04	6.25	<0.05

A round AA7050 bar, with a starting diameter $\Phi = 180$ mm was forged to obtain a first diameter reduction to 75 mm and then, with a multiple hot-forging step, to a final rectangular section shaped plate (70 × 40 mm). The forging cycle was carried out using a 1200-ton press with a hand-forging proprietary cycle. The obtained rectangular section plate underwent a solution treatment, according to AMS2770N, and was water quenched. The proposed process, see Figure 1, was selected because it is representative of a common forging cycle [26] adopted in the production of many aeronautical components—landing gears, connecting rods, rim wheels, etc.—where the ratio between the starting billet section area A_0 and the component final section area A_f is higher than: $A_0/A_f > 9$.

The heat treatment was adopted in agreement with the requirements from the standard AMS2770N, (the fulfillment of this standard is mandatory for AA7050 alloy aeronautical forged component manufacturers) and was completed with room temperature up-setting and final two stages aging (5 h at 394 K + 8 h at 450 K). The two innovative cycles only varied from that required by the standard AMS2770N with regard to the up-setting temperature, carried out at 423 K and 473 K instead of room temperature, while all the other cycle steps were unmodified (Table 2). It must be stated that, in any case, the components manufactured using these innovative cycles, even if they have better performance, cannot be commercialized and utilized for airplane construction.

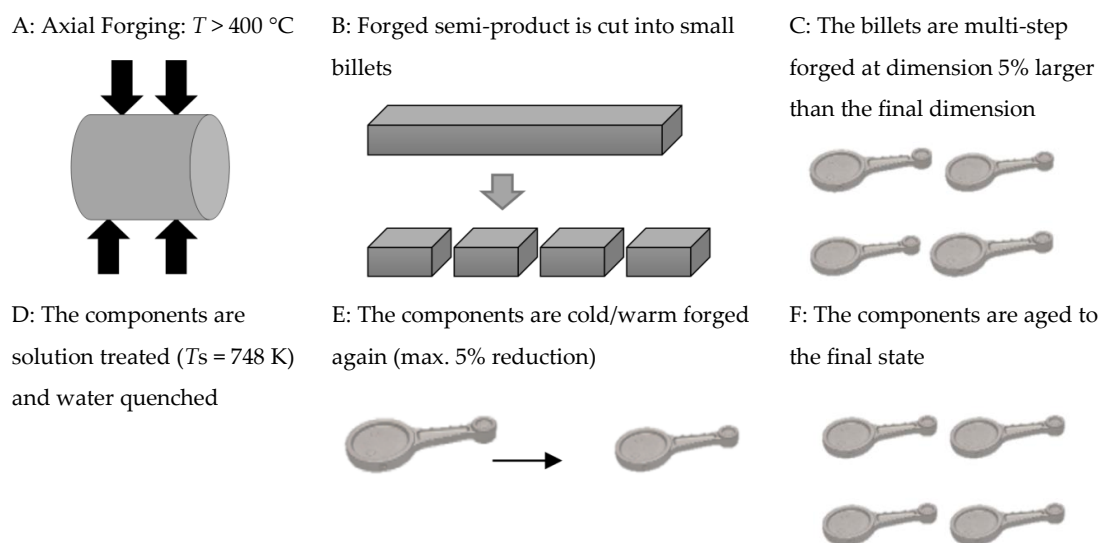


Figure 1. Forging process draft.

Table 2. Standard and modified industrial hot-forging cycle for AA7050 alloy.

Standard Industrial Hot-Forging Cycle (According to AMS2770N)	Modified Industrial Hot Forging Cycle
Total section area reduction: 75%	Total section area reduction: 75%
Solution treatment ($T_s = 748$ K)	Solution treatment ($T_s = 748$ K)
Soaking time: 5 h	Soaking time: 5 h
Water quenching	(fulfills AMS2770N)
Room temperature up-setting: 5% max	Water quenching (fulfills AMS2770N)
Ageing in two steps: 394 K for 5 h + 450 K for 8 h	423 K and 473 K up-setting: 5% max each T
	(does not fulfill AMS2770N)
	Ageing in two steps: 394 K for 5 h + 450 K for 8 h,
	(fulfills AMS2770N)

Tensile tests (mean strain-rate = 0.03 s^{-1} according to ASTM E8) were carried out on the hot-forged and heat-treated AA7050 samples, and Brinell hardness tests and plain strain fracture toughness (KIC) tests were carried out on the transverse specimens (according to the ASTM E399 standard).

Finally, in order to investigate the microstructure, the longitudinal section of the samples was observed, after the standard and innovative cycles, by using a high-resolution Hitachi SU70 SEM (Hitachi High-Technologies Europe, Europark Fichtenhain, Krefeld, Germany), equipped with a Noran 7.0 EBSD system by Thermo-Fischer Scientific (Takkebijsters 1, The Netherlands). EBSD observations were performed using an acceleration voltage of 20 kV after electro-polishing with a solution of 1/3 nitric acid in 2/3 of methanol, at 243 K. Furthermore, EBSD maps were elaborated using MTEX tools in Matlab to highlight grains, crystallographic orientations, grain boundaries and to calculate the average grain size.

The metallographic samples A1, taken from the standard AMS4333 cycle (deformed at $T = 293$ K), A2 and A3, taken from each of the two innovative cycle variations (deformed at $T = 423$ K and 473 K, respectively) were analyzed by mean SEM FEG LEO 1550 ZEISS (McQuairie, London, UK) equipped with an EDS OXFORD X ACT system (v2.2, Oxford Instruments, Abington, UK). Three high magnification (50 KX) metallographic areas were examined for each of the three samples in order to establish a statistical base for the number of quantitative precipitates and the size assessments and analyses. The precipitate counts performed on the SEM-FEG images were carried out by means of IMAGE-J Fiji 1.46 (v1.46, NIH, Bethesda, MD, USA), a software for automatic image processing and analysis.

3. Results and Discussion

The Brinell hardness (HB), yield stress (YS) and ultimate tensile strength (UTS) measured along the transverse (orthogonal direction with respect to the forged cylinders axis) and longitudinal directions (parallel to the forged cylinder axis) as a function of the deformation temperature are shown in Figure 2. The A5 elongations and Z area reduction showed constant values for all the specimens and are not reported. The obtained results for the samples deformed at room temperature represent the reference values (standard process). The laboratory testing characterization permitted us to verify that the mechanical properties investigated were improved by the introduction of the innovative cycle. However, though the tensile properties showed a slight increase of about 2%, the hardness and KIC performance showed a useful improvement. In particular, the innovative process with up-setting at $T = 473$ K led to an enhancement of about 7% of the mean hardness values and 11% mean fracture toughness KIC values (see Figure 2; Figure 3) with respect to the process cycle carried on in agreement with the AMS2770N standard. Furthermore, another interesting result is that the KIC data scatter of the three tests results was significantly reduced after up-setting at 473 K.

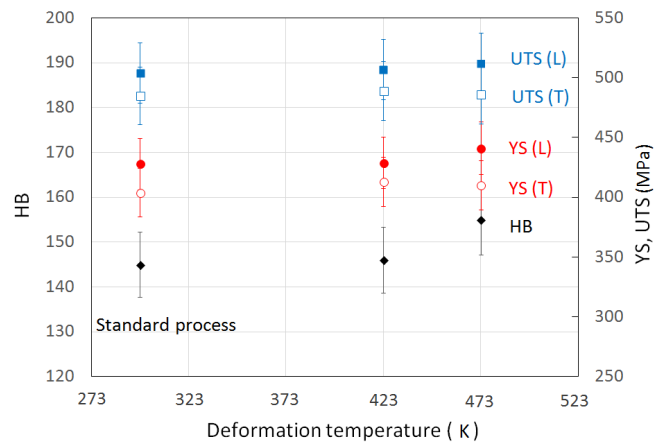


Figure 2. Brinell hardness (BH), yield stress (YS) and ultimate tensile strength (UTS) measured along the transverse (T) and longitudinal (L) directions vs. the deformation temperature of up-setting before ageing (the mean values and data scattering refer to ten measurements for hardness and three tensile tests per condition).

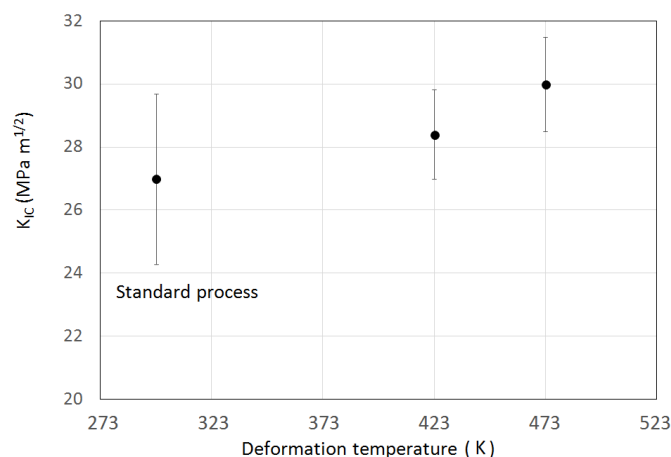


Figure 3. KIC values vs. deformation temperature (mean values for three specimens per condition).

In order to assess the microstructure and precipitation changes introduced by the modified cycles, the characterization of the samples involved both EBSD and SEM-FEG examinations. The EBSD observations performed on the samples deformed at 293 K, 423 K and 473 K (Figure 3) showed

important differences. In Figure 4, the EBSD orientation maps for the grain boundary with 5° misorientation is shown. However, the grains of large size do not exhibit a uniform color, but show areas with darker and/or brighter nuances, indicating the presence of sub-grains with misorientations lower than 5° . It is evident that the warm deformation caused better homogeneity of the refined microstructure. Table 3 indicates the area-weighted average grain size values (d_{wa}) calculated on the obtained maps considering three threshold levels for the grain boundary misorientation angle. The results highlight an actual grain refinement with the increasing up-setting temperature (the d_{wa} value for the Map A1 calculated for the 5° misorientation angle seems to be inconsistent with the observed large grain size. It must be underlined that the grains were not completely embedded into each map, and were not considered to have misled the grain size calculation).

Moreover, the A2 sample (up-setting at 423 K) showed that the size distribution became more homogeneous with a preferred $\langle 111 \rangle$ crystallographic orientation normal to the sample surfaces (blue color in Figure 4b). In addition, in the A3 sample (up-setting at 473 K), the $\langle 111 \rangle$ crystallographic orientation remained in the preferred crystallographic direction (Figure 4c).

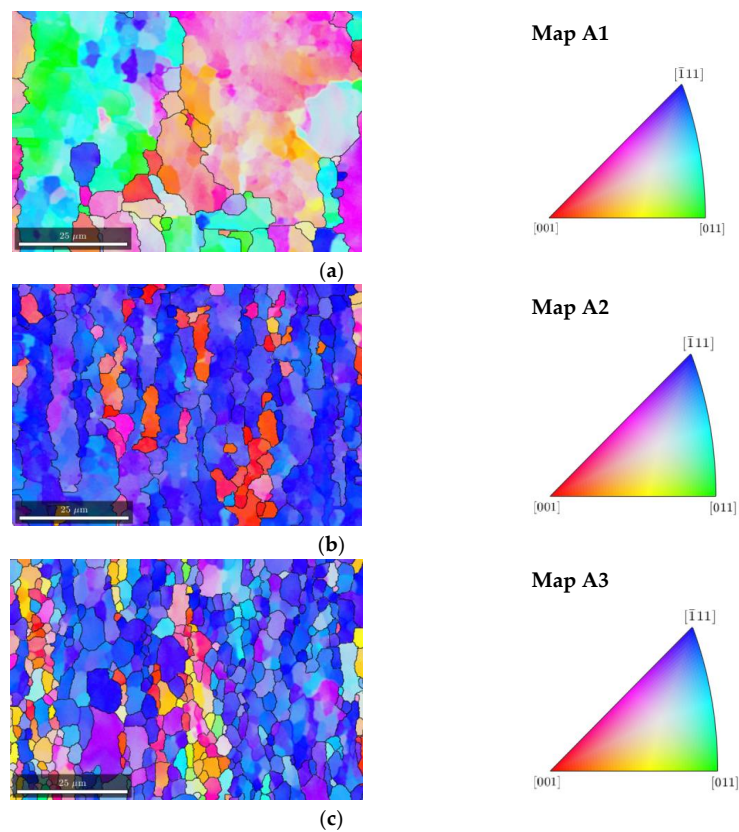


Figure 4. EBSD maps of transversal metallographic sections (belongs to a plane parallel to the forging axis) of samples deformed through up-setting before ageing at: room temperature (a), 423 K (b) and 473 K (c). Black grain boundaries highlight misorientation angles not lower than 5° .

Table 3. Grain sizes calculated on the detected EBSD orientation maps depending on the adopted misorientation angles. The standard deviations are related to the grain size log-norm distribution in the map.

Grain Boundary Misorientation Angle ($^\circ$)	Map A1		Map A2		Map A3	
	d_{wa} (μm)	st. dev.	d_{wa} (μm)	st. dev.	d_{wa} (μm)	st. dev.
1	7.2	0.8	4.9	0.5	4.2	0.4
3	8.4	0.5	7.7	0.4	6.8	0.5
5	9.4	0.6	9.7	0.3	7.1	0.7

The refinement of the microstructure through the thermo-mechanical process has been described in many papers (see e.g., [27–29]), and is termed by some investigators as continuous dynamic recrystallisation (CDR) [21]. The different grain size and orientation evolution in the three examined cases can be tentatively explained by considering the temperature-dependence of dislocation cross-slip. Dislocation cross-slip occurring during a deformation in temperature leads to a general grain re-orientation, and the sub-boundaries present inside the grains evolve towards high-angle boundaries. The higher the deformation temperature, the easier the process. In pure aluminum, thermally-activated dislocation cross-slip has an activation energy of about 14.2 KJ/mole and starts around 423 K.

The scanning electronic microscope SEM-FEG examination of the A1, A2 and A3 samples permitted us to show at least two main precipitate family types, with respect to the size: larger particles at the grain and sub-grain boundaries (mean dimension of 150 nm) and finer nano-sized networks inside the grains and sub-grains (with dimensions up to about 50 nm) (Figure 5). In order to carry out an accurate precipitation population assessment, SEM-FEG images at 50 KX magnification were selected, and some further examination was carried out at 100 KX. It must be reported that it was possible to detect some larger and isolated particles up to 5 μm at grain boundaries, very useful for the chemical analyses.

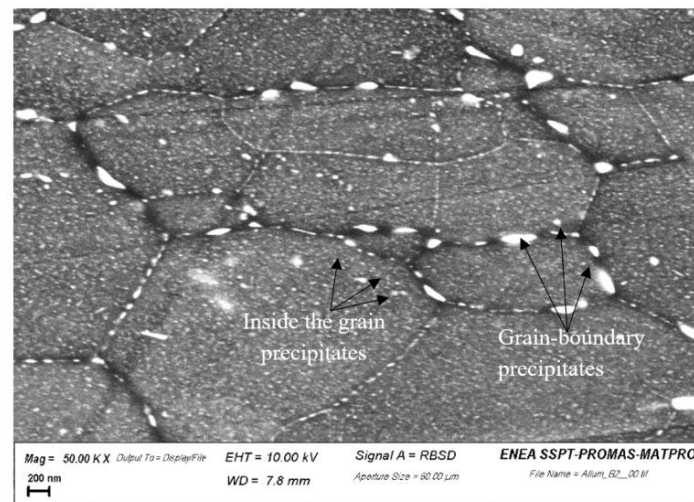


Figure 5. Example of the metallographic microstructure of sample A2 with grain-boundary precipitates (SEM-FEG image).

Each one of the three examined metallographic areas had a dimension of about $6400 \times 4800 \text{ nm}^2$. The maximum distance between the two parallel lines restricting the object in the perpendicular plane to the observation direction was adopted as a Feret diameter. Nine measurements (three measurements of three different areas) per sample (A1, A2 and A3) were carried out to obtain a mean value for the precipitate population in the 50 KX images, and three measurements per sample were carried out for the 100 KX images. The tensile mechanical properties were significantly affected by the additional up-setting in temperature, whilst hardness was affected to a small extent, suggesting that no significant change in fine precipitation occurred. In order to measure the possible evolution of the overall precipitation status, digital image analysis was performed by setting a Feret-diameter threshold of 10 nm. For the A1 sample, we observed 82 precipitates with a Feret-diameter between 10 and 50 nm and only three precipitates with a diameter ranging from 51 and 200 nm.

The comparative measurements of the size of the precipitates for the three specimens are reported in Table 4. The analyses of the results show that the number of precipitates increased as the deformation temperature increased from room temperature up to $T = 473 \text{ K}$. This fact led to the necessity to define a “precipitate areal-density” (defined as the mean value of the number of precipitates detected, including precipitates of all sizes, divided by the constant-reference metallographic area examined, i.e. 6400

nm × 4800 nm). The numbers 82 and 3 were taken as a reference and as base numbers to normalize the other corresponding precipitate quantities in the other samples, in order to represent them as dimensionless ratios to the RT deformed precipitate value (sample A1).

Table 4. SEM-FEG metallographic results (based on nine measurements).

Sample	PR50	PR200
Sample A1 ($T = 293$ K)	1.00	1.00
Sample A2 ($T = 423$ K)	1.59	3.67
Sample A3 ($T = 473$ K)	2.06	4.96

PR50 = Particle ratio of the number of particles detected in the sample with sizes between 10 and 50 nm, divided by the number of particles detected in sample A1 with the same size; PR200 = Particle ratio of the number of particles detected in the sample with sizes between 51 nm and 200 nm divided by the number of particles detected in sample A1 with the same size.

The SEM-FEG equipped with an EDS microprobe was useful to carry out chemical analyses of the larger precipitates in the AA7075 aluminum alloy samples where the Mg-Cu and Mg-Cu-Zn enriched precipitates were detected (Figures 5 and 6). Figure 6 reports the SEM-FEG image of the analyzed sample and Table 5 shows the composition of the examined zones. Figure 7 shows an example of the large Mg + Cu-enriched precipitates revealed by the EDS maps.

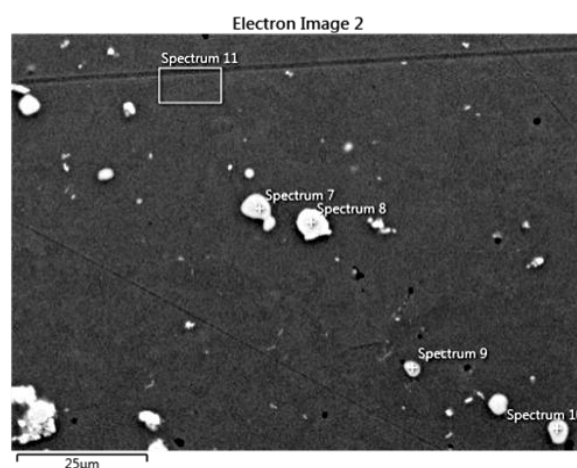


Figure 6. AA7050 alloy zone analyzed using SEM-FEG + EDS point detection.

Table 5. SEM-FEG EDS chemical analysis results (% wt).

Spectrum Label	Al	Mg	Cu	Zn	O	Fe	Ni
7	28.3	21.4	43.5	2.7	4.2	-	-
8	50.2	-	33.4	1.4	-	13.4	1.5
9	62.8	12.1	18.9	3.1	2.7	-	-
10	61.2	16.0	19.6	3.3	-	-	-
11	86.9	4.2	2.1	6.9	-	-	-

The influence of deformation and time on the mechanical properties of 2XXX and 7XXX alloys has been investigated [30] to prove that an increase in the degree of deformation (up to 10%) causes an increase in yield strength and the decrease of tensile elongations. The reason for this improvement is widely discussed in the literature and was found to be related to the microstructure and precipitate evolution mainly formed from GP to Mg(Zn,Cu)₂ phases [31]. Moreover, some authors [30–32] indicate clearly that in AA7050 alloy, an HCP structure phase ($a = 5.32$ Å, $c = 8.79$ Å) nucleates on the grain boundary.

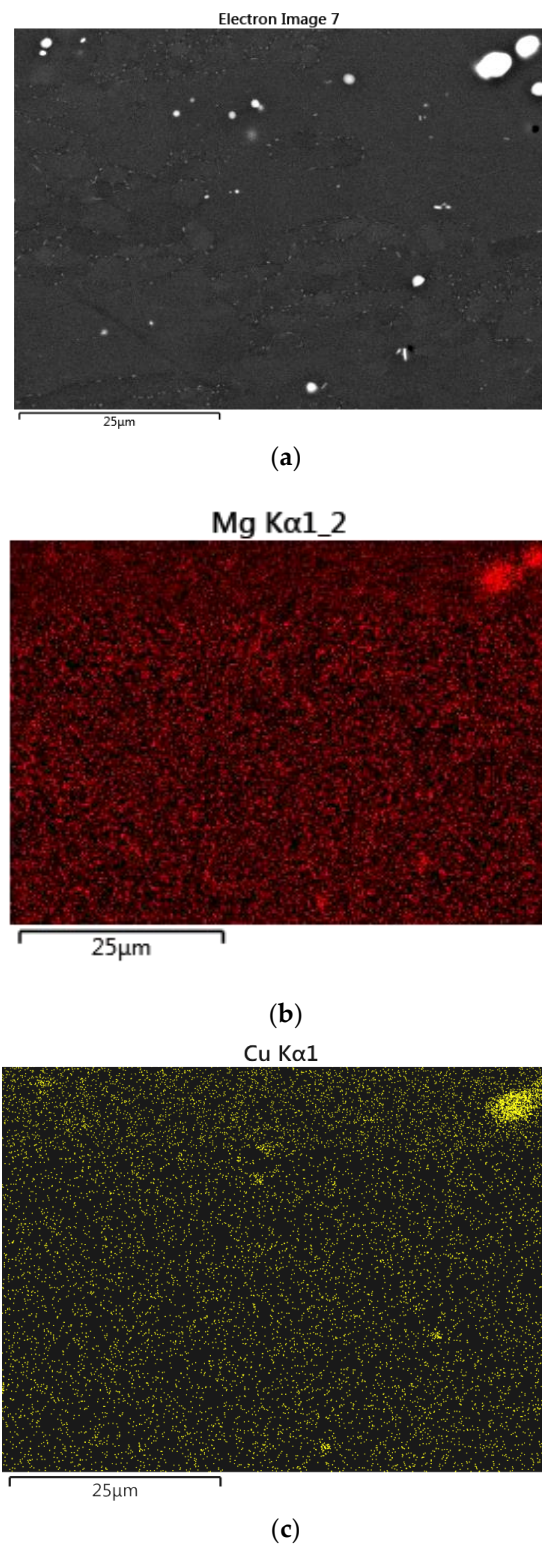


Figure 7. AA7050 alloy zone analyzed (a) with SEM-FEG + EDS area-map scanning of (b) Mg and (c) Cu.

This structure was found to be similar to that of $MgZn_2$ with some Cu next to Mg and Zn. This is an indication that $Mg(Zn,Cu)_2$ was formed with some Zn that was replaced by Cu [32].

Accelerated artificial ageing phenomena have been discussed for the 7XXX families, and [33, 34] have shown that, for Al-Zn-Mg-(Cu) alloys, the η -MgZn₂ phase and η volume fractions are the microstructural features that control the mechanical resistance of the alloys after the ageing treatment.

To optimize the heat treatment, a great deal of efforts have been devoted to finding the optimal conditions, whether one or two stages, with and without a deformation step after solubilization, and a quenching stage. However, no significant improvement in the tensile properties has been found, suggesting that no significant fine precipitation occurs during the unconventional heat and thermo-mechanical treatments proposed here.

Other studies [21,35–38] describe the recrystallisation mechanism of aluminum alloys, confirming the fact that it is crucial to tailor the mechanical properties controlling the grain size and morphology.

Thus, starting from the previous considerations, the current work shows the following main results:

- the warm deformation step included in the heat treatment cycle and replacing the room temperature deformation step refined the grain size and modified the crystallographic orientation in the AA7050 alloy consistently to the CDR, as reported in Figure 3 [21];
- the warm deformation temperature of 473 K resulted in the highest density of large particles with respect to the other two experimental conditions (increased density of large size precipitates in the matrix with a Feret-diameter between 10 and 50 nm, and large size precipitates at the sub-grain boundaries), suggesting a possible over-aging of the alloy during the final heat treatment (394 K for 5 h + 450 K for 8 h, fulfilling AMS2770N);
- the toughness KIC values increased, with a narrower dispersion range value with respect to the standard cycle value dispersion, see Figure 2. The more homogeneous and finer-grained structure obtained after warm deformation contributed to the increased fracture toughness.

The results highlighted that the improvement of the toughness properties should be ascribed to the refinement of the grains and sub-grains developed during warm deformation that were pinned by precipitation during the final heat treatment (394 K for 5 h + 450 K for 8 h, fulfilling AMS2770N). However, because of the precipitation results, which suggested some degree of over-aging, it is likely that some precipitation had already occurred during the warm working and/or, possibly, during subsequent cooling. This is consistent with the preservation of the strength properties. In fact, the loss in strength that normally occurs with over-aging could be compensated by the refinement and pinning of the dislocation structure itself, as it has already been reported in [39,40]. This is consistent with the observed grain refinement in Figure 3 and the higher density of coarse precipitates at the grains and sub-grain boundaries with subsequent warm deformations (Figure 4 and Table 4).

Moreover, Dumont et al. discussed the relationship between the microstructure and toughness in AA7050, [41] and concluded that the coarse intragranular precipitation appeared to play a key role in affecting the toughness as well as the spatial distribution of constituent particles. This conclusion is in line with the results of the present work, where the introduction into the process of a warm deformation step was able to improve the homogeneity of the precipitates, resulting in better toughness values without affecting yield strength.

Finally, even if the modified cycle could be industrially adopted, a criticism may arise as a result of the introduced additional costs. Considering that the introduction of the modified manufacturing cycle requires maintaining a heating furnace at about 473 K (no impact on all the other cycle steps), a marginal extra cost per component is expected. It is very difficult to quantify this extra cost because it depends on the number of components per cycle and on the single component value. Nevertheless, the improvement of the component's safety behavior should also be taken into account to balance the expected extra costs, as already experienced for other classes of materials even with promising properties and performances [42].

4. Conclusions

A warm deformation process of an AA7050 aluminum alloy showed the possibility to increase the fracture toughness behavior with a KIC data dispersion reduction, without significantly affecting the tensile properties. This treatment may be suitable for all the other 7XXX and 8XXX alloy families where a room-temperature deformation step is mandatory for the fulfilment of the international standards.

The adoption of a warm deformation instead of the standard cold deformation (as required by the AMS2770N standard) to reduce material heterogeneity, by producing finer grain and sub-grains pinned by precipitation occurring probably because of over-ageing. It is suggested that the improvement of toughness is related to this improvement in the material microstructure, whilst the tensile properties are unchanged due to the compensation between the flow reduction because of over-ageing and the dislocation structure developed during warm deformation. This process should therefore be applied to forged components with non-uniform thickness characterized by complex 3D shapes that could be easily warm- and not cold-deformed in the intermediate steps between the solution and ageing treatments. No problems are envisaged due to the introduction of the present modifications to thermal treatments, nevertheless, the modified cycle introduces an extra cost due to the re-heating of the components. A preliminary cost-benefit study should be undertaken in order to assess the real economic advantages strictly related to the life applications in service.

The next research steps will focus on the optimization of the precipitation phenomena parameters and the energy for precipitation assessments of other aluminum alloys.

Author Contributions: G.A. and R.D. performed and elaborated the EBSD measurements. C.T. and A.D.S. conceived the experiments and performed SEM observations with EDS. M.R. and A.V. analyze the data. All the authors contributed to and to write the paper.

Funding: This research received no external funding.

Acknowledgments: The authors are grateful to Luciano Pilloni of Enea, CR Casaccia, Italy, for his expertise in SEM-FEG and his appreciated technical suggestions.

Conflicts of Interest: The authors declare no conflict of interest.

References

1. American Society of Materials. *ASM Handbook, Volume 2, Properties and Selection: Nonferrous Alloys and Special Purpose Materials*; ASM International: Materials Park, OH, USA, 2005.
2. Sauvage, X.; Lee, S.; Matsuda, K.; Horita, Z. Origin of the influence of Cu or Ag micro-additions on the age hardening behavior of ultrafine-grained Al-Mg-Si alloys. *J. Alloy. Compd.* **2017**, *710*, 199–202. [[CrossRef](#)]
3. Mondolfo, L.F. *Aluminum Alloys: Structure and Properties*; Butterworth: London, UK, 1976; pp. 497–499.
4. Wang, H.; Yi, Y.; Huang, S. Microstructure Evolution and Mechanical Properties of 2219 Al Alloy during Aging Treatment. *J. Mater. Eng. Perform.* **2017**, *26*, 1475–1482. [[CrossRef](#)]
5. Alunni, A.; Cianetti, F.; Di Schino, A.; Nobili, F.; Richetta, M.; Testani, C. Effect of microstructural parameters on the fatigue behavior for AA2014-T6 alloy. *La Metall. Ital.* **2017**, *5*, 25–31.
6. Scott MacKenzie, D. Heat treating aluminum for aerospace applications. *Heat Treat. Prog.* **2005**, *5*, 37–43.
7. Mott, N.F.; Nabarro, F.R.N. An attempt to estimate the degree of precipitation hardening, with a simple model. *Proc. Phys. Soc.* **1940**, *52*, 86–89. [[CrossRef](#)]
8. Testani, C.; Ielpo, F.M.; Alunni, E. AA2618 and AA7075 alloys superplastic transition in isothermal hot-deformation tests. *Mater. Des.* **2001**, *21*, 305–310. [[CrossRef](#)]
9. Zhao, Y.H.; Liao, X.Z.; Jin, Z.; Valiev, R.Z.; Zhu, Y.T. Microstructures and mechanical properties of ultrafine grained 7075 Al alloy processed by ECAP and their evolutions during annealing. *Acta Mater.* **2004**, *52*, 4589–4599. [[CrossRef](#)]
10. Garay-Reyes, C.G.; Gonzalez, L.; Cuadros-Lugo, E. Correlation between tool flank wear, force signals and surface integrity when turning bars of Inconel 718 in finishing conditions. *Int. J. Adv. Manuf. Technol.* **2017**, *90*, 3045–3053.
11. Pan, L.; Liu, K.; Breton, F.; Chen, X. Effects of minor Cu and Mg additions on microstructure and material properties of 8xxx aluminum conductor alloys. *J. Mater. Res.* **2017**, *32*, 1094–1104. [[CrossRef](#)]

12. *Aerospace Structural Materials Handbook*; DoD, Wright-Patterson Air Force Base: Dayton, OH, USA, 2001.
13. Lu, F.; Zhao, F.; Zhang, J. Heat Treatment of metals. *J. Iron Steel Res.* **2017**, *42*, 144–149.
14. Zhao, F.; Lu, F.; Guo, F. Comparative Analysis of Microstructures and Properties of Two Kinds of Thick Plates of 7050-T7451 Aluminum Alloy. *J. Aeronaut. Mater.* **2015**, *35*, 64–71.
15. Kaibyshev, R.; Sitdikov, O.; Goloborodko, A. Grain refinement in as-cast 7475 aluminum alloy under hot deformation. *Mater. Sci. Eng. A* **2003**, *344*, 348–356. [[CrossRef](#)]
16. Rokni, M.R.; Zarei-Hanzaki, A.; Roostaei, A.; Abedi, H.R. An investigation into the hot deformation characteristics of 7075 aluminum alloy. *Mater. Des.* **2011**, *32*, 2339–2344. [[CrossRef](#)]
17. Li, D.; Zhang, D.; Liu, S.; Shan, Z.; Zhang, X.; Wang, Q.; Han, S. Dynamic recrystallization behavior of 7085 aluminum alloy during hot deformation. *Trans. Nonferr. Met. Soc. China* **2016**, *26*, 1491–1497. [[CrossRef](#)]
18. Sanchez, J.M.; Rubio, E.; Alvarez, M.; Sebastian, M.A.; Marcos, M. Microstructural characterization of material adhered over cutting tool in the dry machining of aerospace aluminium alloys. *J. Mater. Process. Technol.* **2005**, *164–165*, 911–918. [[CrossRef](#)]
19. Prasad, N.E.; Wanhill, R.J. *Aerospace Materials and Material Technologies, Volume 1: Aerospace Materials*; Springer: Singapore, 2017; pp. 29–52.
20. Adam, K.F.; Long, Z.; Field, D.P. Analysis of Particle-Stimulated Nucleation (PSN)-Dominated Recrystallization for Hot-Rolled 7050 Aluminum Alloy. *Metall. Mater. Trans. A* **2017**, *48*, 2062–2076. [[CrossRef](#)]
21. Maizza, G.; Pero, R.; Richetta, M.; Montanari, R. Continuous dynamic recrystallization (CDRX) model for aluminum alloys. *J. Mater. Sci.* **2018**, *53*, 4563–4573. [[CrossRef](#)]
22. Parker, C.G.; Field, D.P. Observation of Structure Evolution during Annealing of 7xxx Series Al Deformed at High Temperature. In *Light Metals 2012*; Springer: Cham, Switzerland, 2012; pp. 383–386.
23. Wang, S.; Luo, J.; Hou, L.; Zhang, J.; Zhuang, L. Physically based constitutive analysis and microstructural evolution of AA7050 aluminum alloy during hot compression. *Mater. Des.* **2016**, *107*, 277–289. [[CrossRef](#)]
24. Angella, G.; Bassani, P.; Tuissi, A.; Vedani, M. Intermetallic particle evolution during ECAP processing of a 6082 alloy. *Mater. Trans.* **2004**, *45*, 2182–2186. [[CrossRef](#)]
25. Angella, G.; Bassani, P.; Tuissi, A.; Ripamonti, D.; Vedani, M. Microstructure evolution and aging kinetics of Al-Mg-Si and Al-Mg-Si-Sc alloys processed by ECAP. *Mater. Sci. Forum* **2006**, *503–504*, 493–498. [[CrossRef](#)]
26. Sabroff, A.M.; Boulger, F.W.; Henning, H.J.; Spretnak, F.W. *A Manual on Fundamentals of Forging Practice*; Battelle Memorial Institute: Columbus, OH, USA, 1971.
27. Gourdet, S.; Montheillet, F. Effects of dynamic grain boundary migration during the hot compression of high stacking fault energy metals. *Acta Mater.* **2002**, *50*, 2801–2812. [[CrossRef](#)]
28. McQueen, H.J. Development of dynamic recrystallization theory. *Mater. Sci. Eng. A* **2004**, *387–389*, 203–208. [[CrossRef](#)]
29. Humphreys, F.J.; Hatherly, M. *Recrystallization and Related Annealing Phenomena*, 2nd ed.; Elsevier: Amsterdam, The Netherlands, 2004.
30. Wyss, R.K. Method for Increasing the Strength of Aluminium Alloy Products through Warm Working. U.S. Patent US005194102A, 16 March 1993.
31. Jarzebska, A.; Bogucki, R.; Bieda, M. Influence of degree of deformation and aging time on mechanical properties and microstructure of aluminium alloy with zinc. *Arch. Metall. Mater.* **2015**, *60*, 215–221. [[CrossRef](#)]
32. De Hass, M.; De Hosson, J.T.M. Grain Boundary segregation and precipitation in aluminium alloys. *Scr. Mater.* **2001**, *44*, 281–286. [[CrossRef](#)]
33. Ber, L.B. Accelerated artificial regimes of commercial aluminium alloys II: Al-Cu, Al-Zn-Mg-(Cu), Al-Mg-Si-(Cu) alloys. *Mater. Sci. Eng. A* **2000**, *280*, 91–96. [[CrossRef](#)]
34. Lang, Y.; Cui, H.; Cai, Y.; Zhang, J. Evolution of nanometer precipitates in AA7050 alloy subjected to overaging treatment and warm deformation. In *Proceedings of the 13th International Conference on Aluminum Alloys (ICAA13)*, Pittsburgh, PA, USA, 3–7 June 2012; Weiland, H., Rollett, A.D., Cassada, W.A., Eds.; Springer: Cham, Switzerland, 2012; pp. 1223–1226.
35. Zuo, J.; Hou, L.; Shi, J.; Cui, H.; Zhuang, L.; Zhang, J. Effect of deformation induced precipitation on grain refinement and improvement of mechanical properties AA 7055 aluminium alloy. *Mater. Charact.* **2017**, *130*, 123–134. [[CrossRef](#)]
36. *Standard AMS 2770N “Heat Treatment of Wrought Aluminium Alloy Parts”*; SAE Aerospace: Warrendale, PA, USA, 2015.

37. Voncina, M.; Medved, J.; Mrvar, P. Energy of precipitation of Al_2Cu and $\alpha-AlFeSi$ phase from the $AlCu_3$ alloy and the shape of precipitates. *Metalurgija* **2009**, *48*, 9–13.
38. Mandal, P.K. Study on hardening mechanisms in aluminium alloys. *Int. J. Eng. Res. Appl.* **2016**, *6*, 91–97.
39. Paton, N.E.; Sommer, A.W. *Proceedings of 3rd International Conference on Strength of Metals and Alloys*; Metals Society: London, UK, 1973; Volume 1.
40. Polmear, I.J. *Light Alloys*, 3rd ed.; Arnold Ed: London, UK, 1995.
41. Dumont, D.; Deschamps, A.; Brechet, Y. On the relationship between microstructure, strength and toughness in AA7050 aluminium alloy. *Mater. Sci. Eng. A* **2003**, *356*, 326–336. [[CrossRef](#)]
42. Astarita, A.; Testani, C.; Scherillo, F.; Squillace, A.; Carrino, L. Beta Forging of a Ti6Al4V Component for Aeronautic Applications: Microstructure Evolution. *Metallogr. Microstruct. Anal.* **2014**, *3*, 460–467. [[CrossRef](#)]



© 2019 by the authors. Licensee MDPI, Basel, Switzerland. This article is an open access article distributed under the terms and conditions of the Creative Commons Attribution (CC BY) license (<http://creativecommons.org/licenses/by/4.0/>).